



# Exploring the applicability of amorphous films of system In-Sb-Te as phase change materials



Vitaliy Bilovol, Bibiana Arcondo \*

INTECIN, Universidad de Buenos Aires – CONICET, Facultad de Ingeniería, Laboratorio de Sólidos Amorfos, Paseo Colon 850, C1063ACV Buenos Aires, Argentina

## ARTICLE INFO

### Article history:

Received 6 April 2016

Received in revised form 10 June 2016

Accepted 12 June 2016

Available online xxxx

### Keywords:

Chalcogenides

In-Sb-Te

Films

Electrical resistivity

Phase change memory

## ABSTRACT

Hereby, we present In-Sb-Te amorphous films grown by pulsed laser deposition technique using, as targets, crystalline ingots (with corresponding stoichiometry) prepared by traditional melt-quenching method. The explored nominal compositions were  $\text{In}_{50}\text{Sb}_{15}\text{Te}_{35}$ , about a ternary compound formed in the quasi-binary InTe-SbTe system, metastable at room temperature, and two eutectics  $\text{In}_8\text{Sb}_8\text{Te}_{84}$  and  $\text{In}_{10}\text{Sb}_{51}\text{Te}_{39}$ . Measurements of electrical sheet resistance evidenced that the amorphous films behave as electrical insulators at room temperature and present a giant jump in resistivity towards a conducting state on crystallization. Differential scanning calorimetry technique complemented the structural information obtained by X-ray diffraction and revealed temperatures of crystallization of the amorphous films as well as their melting points. Due to their temperature characteristics (crystallization temperature  $\approx 225$  °C and melting temperature  $\approx 540$  °C),  $\text{In}_{10}\text{Sb}_{51}\text{Te}_{39}$  film results very attractive from technological point of view. These characteristics could make this eutectic composition a good candidate for using in phase-change memory devices.

© 2016 Elsevier B.V. All rights reserved.

## 1. Introduction

Since the early sixties, chalcogenide glasses called the attention of many researchers due to their ability, exhibited in chalcogenide films, to change between two states with remarkable different properties (reflectivity or resistance) upon the application of a laser shot or a current pulse [1,2,3,4]. The best technique to obtain glasses in any geometry, for a certain application, depends on the composition of the starting material and is still under continuous development.

In the case of 2D geometry (thin films), the most frequently employed techniques are evaporation [5], sputtering [6], spin coating [7] and pulsed laser deposition (PLD) [8]. Evaporated films do not maintain the composition of the starting chalcogenide material even using flash evaporation. This problem is overcome by sputtering but, however, the films obtained by this technique may present a columnar morphology [9]. Spin coating is mentioned as a low cost technique that retains glass stoichiometry and high film quality [10]. On the other hand, the need of solvents for the film deposition leaves an amount of residual solvent, whose presence leads to variation in the optical properties of the films. Pulsed laser deposition is a very versatile technique that lets the obtaining of films that show a smooth morphology and uniform thickness without changing appreciably the target composition.

Until now there are basically two classes of phase change materials in technological applications: the more widely used germanium antimony telluride [11] and indium antimony telluride based [12] materials. These materials have already been employed in optical discs such as CDs, DVDs and Blue-ray Discs since 1994 for Ge-Se-Te and 1997 for Ag-In-Sb-Te [13]. However, as the pronounced property contrast between amorphous and crystalline states is not only optical but also electrical, their rapid switching speed might also enable a very fast, non-volatile electronic memory.

In-Sb-Te system presents, as well as Ge-Sb-Te, a pseudo-binary alloy along InSb-InTe tie line [13] but in spite that InSb and InTe are characterised by tetrahedral nearest-neighbor environments for the cation, this pseudo binary alloy,  $\text{In}_3\text{SbTe}_2$  (IST), has metastable rock salt structure [14] with octahedral In environments. Moreover, whereas for  $\text{Ge}_2\text{Sb}_2\text{Te}_5$  (GST) the cation network (Ge, Sb) is disordered [15], in  $\text{In}_3\text{SbTe}_2$  the disordered network is the anion one (Sb,Te) [14]. On the other hand IST is stable at higher temperatures than GST and their crystallizations proceed following different stages presenting, each one, a characteristic resistivity. [16] Their transport properties also differ. Crystalline IST is metallic but it is semiconductor when it is amorphous [14] whereas GST is semiconductor in both cases.

Samples away from InSb-InTe tie line have also been studied.  $\text{In}_{15}\text{Sb}_{43}\text{Te}_{42}$ ,  $\text{In}_{24}\text{Sb}_{38}\text{Te}_{38}$  and  $\text{In}_{47}\text{Sb}_{14}\text{Te}_{39}$  samples, prepared by D.C. magnetron sputtering, were evaluated by Liqui Men et al. [4] who found crystallization temperatures of 240, 246 and 305 °C respectively for a heating rate of 20 °C/m. They conclude that the composition

\* Corresponding author.

E-mail address: [barcond@fi.uba.ar](mailto:barcond@fi.uba.ar) (B. Arcondo).

$\text{In}_{47}\text{Sb}_{14}\text{Te}_{39}$ , which crystallization products consisted of  $\text{In}_3\text{SbTe}_2$ ,  $\text{In}_2\text{Te}_3$  and  $\text{InTe}$ , possesses higher activation energy and is more stable than those of the other compositions. More recently, Hromadko et al. [17] analyzed samples of the  $\text{Sb}_{70-x}\text{In}_x\text{Te}_{30}$  ( $x = 0, 7, 14$  at.%) system prepared by flash thermal evaporation. They found that, by thermal annealing, all samples crystallize in a single exothermic peak. Samples with lower  $x$  crystallize in rhombohedral Kifune structures [18] whereas for  $x = 14$  crystallize in a structure similar to rhombohedral Sb. They also found that the difference of electrical sheet resistance between amorphous and crystalline state is more than 3 orders of magnitude and that the samples containing indium evidenced higher crystallization temperature and activation energies of crystallization.

The purpose of this paper is to deepen the research of the potentiality for the application in PCM of films obtained by means of PLD from targets of ternary In-Sb-Te system. Particularly, we explored thermal and electrical characteristics of films of two ternary eutectic compositions,  $\text{In}_8\text{Sb}_8\text{Te}_{84}$  (E1) and  $\text{In}_{10}\text{Sb}_{51}\text{Te}_{39}$  (E2), in addition to films of composition  $\text{In}_{50}\text{Sb}_{15}\text{Te}_{35}$ , about the well-known ternary compound  $\text{In}_3\text{SbTe}_2$  (IST), and bulk samples of the corresponding stoichiometries. The evaluation of eutectic compositions is aimed by the following facts i) In-Sb-Te system exhibits extended ranges of solid state solubility, ii) eutectic crystallization, if this were the case, would occur in a single exothermic reaction increasing the crystallization rate relative to that of multi-phase samples and iii) the eutectic solidification may favor multicomponent samples amorphization.

## 2. Experimental

In-Sb-Te ingots were obtained by the melt quenching procedure of a mixture of the elemental components, enclosed in previously evacuated quartz ampoules, heated for 8 h at 950 °C. The thin films were prepared by laser ablation of the targets, made with ingot pieces, employing a pulsed Nd-YAG laser radiation of  $\lambda = 355$  nm.

Thermal characterization was performed in a Differential Scanning Calorimeter (DSC) Perkin Elmer Pyris 1. In the case of the film characterizations, they were scraped off the substrate, whereas bulk samples were powdered. Calorimetric curves were recorded with a heating rate of 40 °C/min. Samples were sealed into aluminum/copper capsules and measured under Ar flow from room temperature, RT, up to the melting point,  $T_m$ .

Electrical characterization, consisting in the measurements of sheet resistance  $R_s$  as a function of temperature, was performed on films heated inside a dark evacuated chamber. The sheet resistance was measured with two contacts, separated for about 3 mm, in a Keithley 617 electrometer whereas temperature was measured with a thermo-resistance Pt100 in contact with the film. Heating rate employed was about 30 °C/min.

Structure characterization was performed by X-Ray Diffractometry (XRD) in a  $\theta$ - $2\theta$  diffractometer with monochromatized  $\text{Cu-K}\alpha$  radiation. Bulk samples were measured in powder form whereas films were measured on standard microscope glass substrates. The crystalline phases were identified using the international data base JCPDS-ICDD. XRD film characterizations were performed on virgin films, on films submitted to DSC scans and also on films submitted to electrical measurements. Additionally,  $\text{Sb}_2\text{Te}_3$  was synthesized as a reference sample, using the melt quenching technique. After that, XRD of the powdered sample was carried out. The pattern was analyzed with MAUD software [19] and the fitting parameters of the unit cell were extracted in order to calculate the lattice volume.

## 3. Results and discussion

### 3.1. Structure analyses and thermal behavior of bulk materials and films

#### 3.1.1. $\text{In}_{50}\text{Sb}_{15}\text{Te}_{35}$

Fig. 1A shows XRD pattern of  $\text{In}_{50}\text{Sb}_{15}\text{Te}_{35}$  sample. As it can be seen, the sample obtained by melt-quenching method is crystalline.

The cooling rate was not enough to avoid crystallization evidencing a poor capacity of the system to form bulk glasses. The identified phases were tetrahedral  $\text{InTe}$  (PDF#30-0636,  $I4/mcm$ ), cubic  $\text{InSb}$  (PDF#06-0208,  $F-43m$ ) and cubic  $\text{In}_3\text{SbTe}_2$  (PDF#17-0849,  $Fm3m$ ).

In accordance to the equilibrium phase diagram [20],  $\text{In}_3\text{SbTe}_2$  is peritectically formed upon cooling at nearly 555 °C and decomposes into  $\text{InSb}$  and  $\text{InTe}$  below 420 °C. In our case, the cooling rate was fast enough to avoid a full decomposition of IST phase, but it was too slow to get an amorphous ingot. Fig. 1B shows DSC curve of  $\text{In}_{50}\text{Sb}_{15}\text{Te}_{35}$  powdered sample. The curve exhibits some endothermic transitions without any evidence of crystallization of the sample (no exothermic reaction). The endothermic peaks could be interpreted, in agreement with the equilibrium phase diagram, [20] as follows. The first peak at 437 °C in the DSC heating curve corresponds to the formation of  $\text{In}_3\text{SbTe}_2$  from the solid state reaction of binary  $\text{InSb}$  and  $\text{InTe}$  whose presence was already observed in  $\text{In}_{50}\text{Sb}_{15}\text{Te}_{35}$  XRD pattern. The 511 °C peak may be attributed to the melting point of the quasi binary eutectic formed by 15 mol%  $\text{In}_3\text{SbTe}_2$  and 85 mol%  $\text{InSb}$  [21], that coexists with solid  $\text{In}_3\text{SbTe}_2$  compound. The eutectic temperature reported in [21] is 512 °C, not far from the 508 °C reported in [20]. The 556 °C peak is attributed to the peritectic transformation of the remaining  $\text{In}_3\text{SbTe}_2$  into a liquid of composition about 60 mol%  $\text{InSb}$ , and solid  $\text{InTe}$ , reported in the quasibinary section in the ternary system. The peritectic temperature reported by [21] is 568 °C whereas that reported by [20] is 555 °C.

Fig. 2A shows the XRD pattern of the  $\text{In}_{50}\text{Sb}_{15}\text{Te}_{35}$  film together with the substrate pattern. These patterns may be attributed to non-crystalline structures as was confirmed by scanning electron microscopy. The average composition of the film deposited on a Si wafer, as was determined by energy dispersive X-ray spectroscopy (EDX), is  $\text{In}_{50.83}\text{Sb}_{16.97}\text{Te}_{32.20}$ .

The main features of constant rate heating DSC curve of  $\text{In}_{50}\text{Sb}_{15}\text{Te}_{35}$  film (Fig. 2B) are two exothermic peaks at about 302 °C and 320 °C. These may be unambiguously attributed to the crystallization of  $\text{InSb}$  and  $\text{InTe}$  phases, respectively. The  $\text{InSb}$  crystallization temperature ( $T_c$ ) agrees very well, whereas the  $\text{InTe}$   $T_c$  is rather low compared with

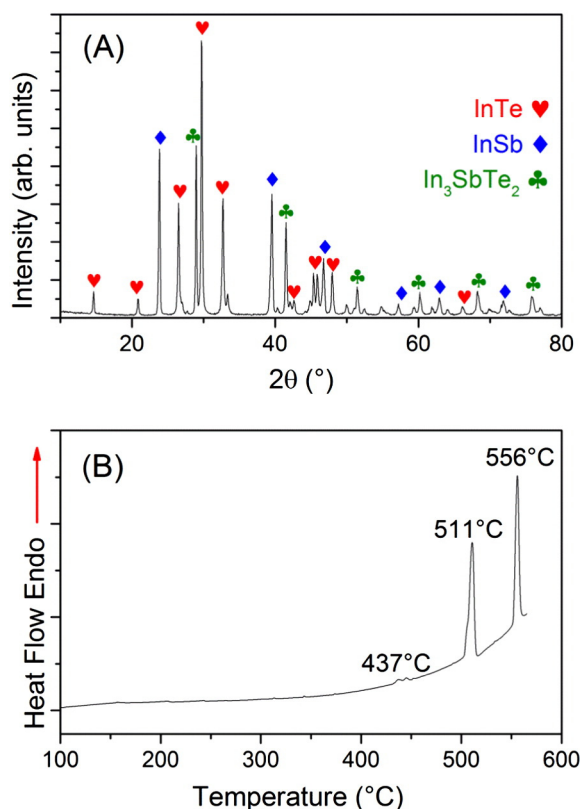
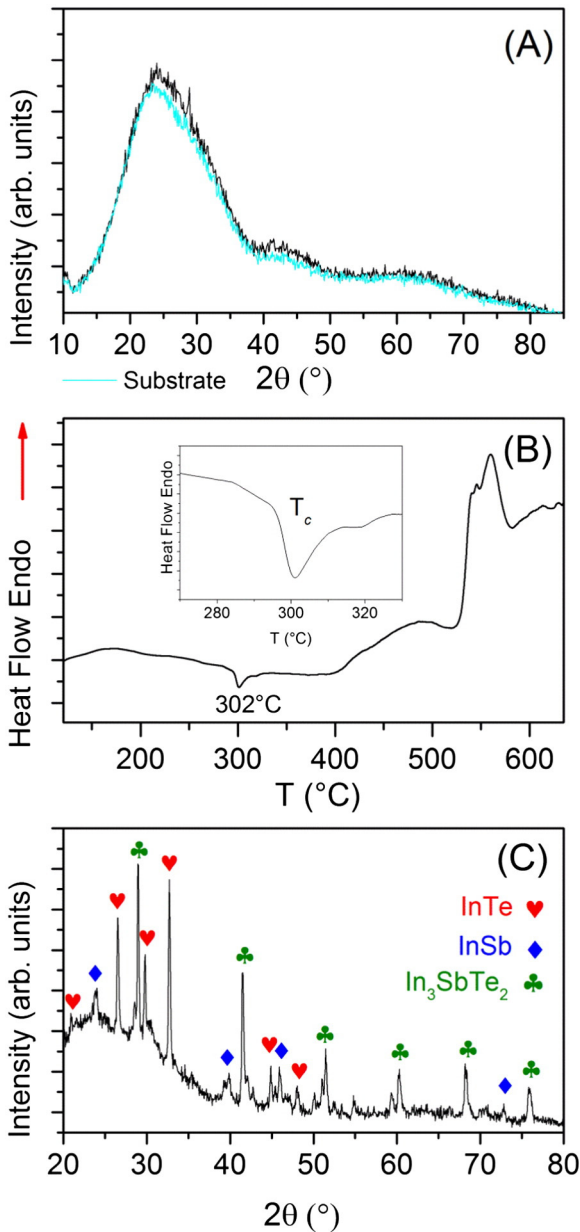


Fig. 1.  $\text{In}_{50}\text{Sb}_{15}\text{Te}_{35}$  ingot. A) XRD and B) DSC heating curve.



**Fig. 2.** A) XRD patterns of as made  $\text{In}_{50}\text{Sb}_{15}\text{Te}_{35}$  film and the substrate as a reference; B) DSC curve of as made  $\text{In}_{50}\text{Sb}_{15}\text{Te}_{35}$  film; C) XRD after DSC measurement of  $\text{In}_{50}\text{Sb}_{15}\text{Te}_{35}$  film.

the one reported by Kim et al. [22] (350 °C) for the crystallization of a film with the same chemical composition but prepared by co-sputtering method. Increasing temperature above 400 °C, a change of thermal behavior can be observed. Unlike the bulk sample, the film with the same nominal composition exhibits a very spread endothermic hump in the temperature range of 420–520 °C, probably corresponding to the formation of  $\text{In}_3\text{SbTe}_2$  and the following eutectic melting transformation. Finally, the endothermic signal in the 530–570 °C temperature range may be associated to the peritectic transformation, in correspondence to the endothermic peak already observed for bulk sample at 555 °C. The XRD analysis of the  $\text{In}_{50}\text{Sb}_{15}\text{Te}_{35}$  film (Fig. 2C) performed after DSC scan, shows the crystalline products of  $\text{In}_{50}\text{Sb}_{15}\text{Te}_{35}$  solidification. Three phases (InTe, InSb and  $\text{In}_3\text{SbTe}_2$ ) are identified.

### 3.1.2. $\text{In}_8\text{Sb}_8\text{Te}_{84}$ (E1)

According to XRD pattern, as made melt-quenched sample E1 resulted highly crystallized, corroborating the marginal glass forming ability

of this system. From the diffractogram, hexagonal Te (PDF#36-1452,  $P3_121$ ), as the main phase, rhombohedral  $\text{Sb}_2\text{Te}_3$  (with  $\text{In}_2\text{Te}_3$  as a solute) (PDF#15-0874,  $R-3m$ ) and cubic  $\text{In}_2\text{Te}_3$  (PDF#33-1488,  $F-43m$ ) crystalline phases were identified. Rhombohedral  $\text{Sb}_2\text{Te}_3$  with  $\text{In}_2\text{Te}_3$  as a solute will be called  $\text{In}_x\text{Sb}_{2-x}\text{Te}_3$ . The dominant content of Te is in agreement with the nominal composition of the eutectic E1. Nevertheless,  $\text{In}_2\text{Te}_5$ , that is an equilibrium phase expected in E1 [20] was not observed and  $\text{In}_2\text{Te}_3$  was identified in its place. This may be attributed to the fact that  $\text{In}_2\text{Te}_5$  is peritectically formed as will be discussed later. As in the case of  $\text{In}_{50}\text{Sb}_{15}\text{Te}_{35}$  film, E1 film obtained by PLD resulted to be amorphous (Fig. 3A). The average composition of E1 film measured by EDX is  $\text{In}_{8.39}\text{Sb}_{8.28}\text{Te}_{83.33}$ .

DSC heating scan of E1 film is shown in Fig. 3B. An exothermic signal at about 145 °C may be attributed to the crystallization of the film. While the endothermic signal at about 400 °C is in agreement with the eutectic melting point reported by Legendre [20]. After the DSC thermal scan, the XRD pattern of the crystalline film (Fig. 3C) shows the presence of Te as the main phase and  $\text{In}_x\text{Sb}_{2-x}\text{Te}_3$  but neither  $\text{In}_2\text{Te}_3$  nor  $\text{In}_2\text{Te}_5$  were detected.

### 3.2. $\text{In}_{10}\text{Sb}_{51}\text{Te}_{39}$ (E2)

E2 eutectic ingot obtained by melt quenching procedure is also crystalline. The main phases identified in the XRD pattern are  $\text{In}_x\text{Sb}_{2-x}\text{Te}_3$  and InSb, probably with certain amount of rhombohedral Sb (PDF#35-0732,  $R-3m$ ) as well. According to the equilibrium phase diagram [20], eutectic E2 should be formed by  $\text{In}_x\text{Sb}_{2-x}\text{Te}_3$ , Sb and  $\text{In}_2\text{Te}_3$ . However, no fingerprints of  $\text{In}_2\text{Te}_3$  are observed in X-ray diffractograms within the technique's threshold.

The average composition of amorphous E2 film (See Fig. 4) measured by EDX is  $\text{In}_{10.34}\text{Sb}_{52.44}\text{Te}_{37.22}$ . DSC scan of E2 film reveals an exothermic peak (224 °C), attributed to crystallization. An endothermic peak is observed at 363 °C and a second endothermic peak at 542 °C that may be attributed to the melting point of this eutectic. This temperature is in a good agreement with that (535 °C) reported in [20]. After DSC scan, XRD pattern shows  $\text{In}_x\text{Sb}_{2-x}\text{Te}_3$ , Sb should also be present.

### 3.3. Temperature dependence of films resistance

Fig. 5 collects the results of the temperature-dependent sheet electrical resistivity ratio  $\rho_r = R_s/R_0$  with  $R_0$  the resistance of the amorphous film at RT. From top to bottom  $\rho_r(T)$  curves on  $\text{In}_{50}\text{Sb}_{15}\text{Te}_{35}$ , E1 and E2 films are depicted. Starting the experiments at RT,  $\rho_r$  decreases smoothly with increasing temperature evidencing a semiconductor behavior for the amorphous films. The abrupt decrease of  $\rho_r$  with increasing temperature corresponds to an amorphous-to-crystalline transition in the films (4–7 orders of magnitude).

In general, the behavior of the electrical resistance can be correlated with DSC data. The  $T_c$  from the DSC curves are somewhat higher (5–20 °C) than the ones from the resistance measurements. It may be attributed to the fact that we carried out the DSC measurements with a higher velocity (40 °C/min) than the  $R_s$  measurements (about 30 °C/min). We also want to mark that the XRD patterns of the samples performed after DSC result notoriously more crystalline than those obtained after  $R_s(T)$  experiments. This may be attributed to the fact that at the end of DSC scans the samples melt and recrystallize, on cooling, inside the capsule installed in the DSC holder whereas  $R_s(T)$  measurements finish just several degrees after crystallization, much before the melting point.

$\rho_r(T)$  of  $\text{In}_{50}\text{Sb}_{15}\text{Te}_{35}$  film, shown in Fig. 5A, presents two features associated to crystallization, one at 303 °C that may be associated to the beginning of InSb crystallization and a more pronounced one at 320 °C that may be associated to the beginning of InTe crystallization. These temperatures agree with those obtained by DSC. However, a remarkable change in  $\rho_r$  takes place at higher temperature, about 370 °C. This jump may be associated to the percolation of the crystalline phases. In

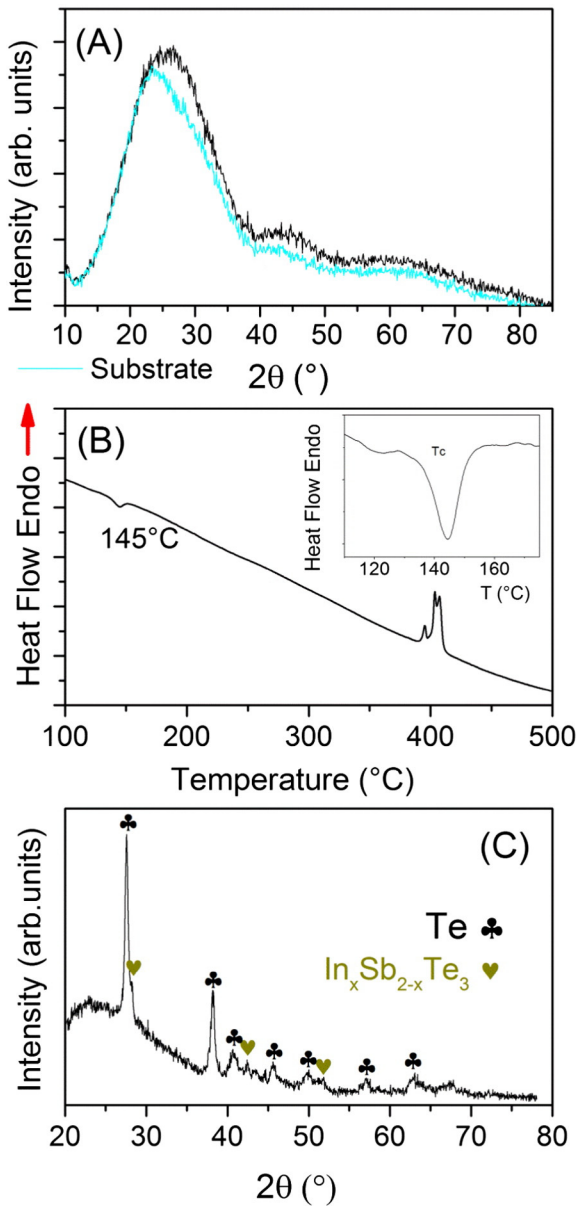


Fig. 3. A) XRD pattern of as made E1 film, B) Thermal DSC scan of E1 film, C) XRD pattern of E1 film after DSC scan.

agreement with these results, XRD patterns obtained after  $R_s$  measurements depicted in Fig. 6A, show InSb, InTe and only traces of  $\text{In}_3\text{SbTe}_2$ . Additionally, a single wide peak whose position coincides with (511) peak of  $\text{In}_2\text{Te}_3$  is observed.

The free cooling of the sample is performed inside the measurement chamber and was also registered. As is observed in Fig. 5A, the crystallized  $\text{In}_{50}\text{Sb}_{15}\text{Te}_{35}$  film is semiconductor and the temperature dependence of  $\rho_r$  is very smooth.

From the Arrhenius plot shown in the inset, a slope of  $-0.71$  eV was determined for amorphous  $\text{In}_{50}\text{Sb}_{15}\text{Te}_{35}$ . That is, an activation energy for electric transport  $E_G = 0.71$  eV. Samples heated up to higher temperatures (i.e.  $480^\circ\text{C}$ ) exhibit additional features, particularly a change of slope from about  $404^\circ\text{C}$  to  $439^\circ\text{C}$  that may be attributed to the solid state reaction forming  $\text{In}_3\text{SbTe}_2$  and a change, on heating, from semiconductor to metallic transport regime, proper of crystalline IST, at  $452^\circ\text{C}$  (inset of Fig. 5A).

$\rho_r(T)$  of E1 film depicted in Fig. 5B presents a fall of two orders of magnitude at about  $135^\circ\text{C}$  that may be attributed to crystallization. At about  $150^\circ\text{C}$  a change of slope is observed towards a slope not far

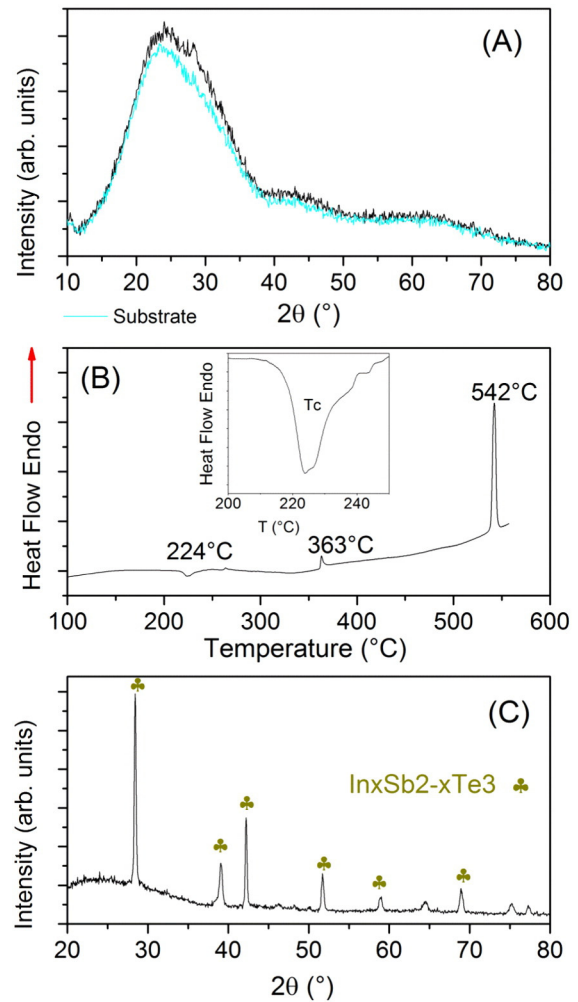


Fig. 4. A) XRD pattern of as made E2 film, B) Thermal DSC heating scan of E2 film, C) XRD pattern of E2 film after DSC scan.

from that corresponding to the amorphous film. From this point, no other significant transformation is observed until the heating is interrupted at about  $230^\circ\text{C}$ .

Along the free cooling process, a change of slope is registered. At higher temperature a metallic behavior dominates whereas below  $160^\circ\text{C}$ , the sample shows semiconducting behavior with a smooth dependence of  $\rho_r$  on temperature.

From the Arrhenius plot shown in the inset, the activation energy of electric conduction in the amorphous film is determined as  $E_G = 0.30$  eV.

According to XRD patterns, depicted in Fig. 6B, obtained after measurements of  $R_s(T)$ , the only crystallization product, attained in the measurement temperature range, is Te. Nevertheless, from the analyses of Te pattern depicted in Fig. 6B, a volume contraction of about 2% relative to the cell volume corresponding to hexagonal Te (PDF#36-1452) and also to Te pattern depicted in Fig. 3C, was determined. This volume contraction may be due to the presence of In and Sb solutes in Te structure.

$\rho_r(T)$  of E2 film, shown in Fig. 5C, presents a change of slope at  $173^\circ\text{C}$  which continues in a steep fall of about three orders of magnitude at about  $197^\circ\text{C}$  that may be associated to crystallization. The feature at  $173^\circ\text{C}$  may be an artifact attributed to a change in the constant heating rate. At  $210^\circ\text{C}$  a change of slope takes place but, at about  $260^\circ\text{C}$ , the slope decreases once more leaving  $\rho_r(T)$  nearly constant. Once the heating is interrupted at about  $290^\circ\text{C}$ ,  $\rho_r(T)$  remains constant up to  $200^\circ\text{C}$  but below this temperature the resulting behavior of  $\rho_r(T)$  is metallic.

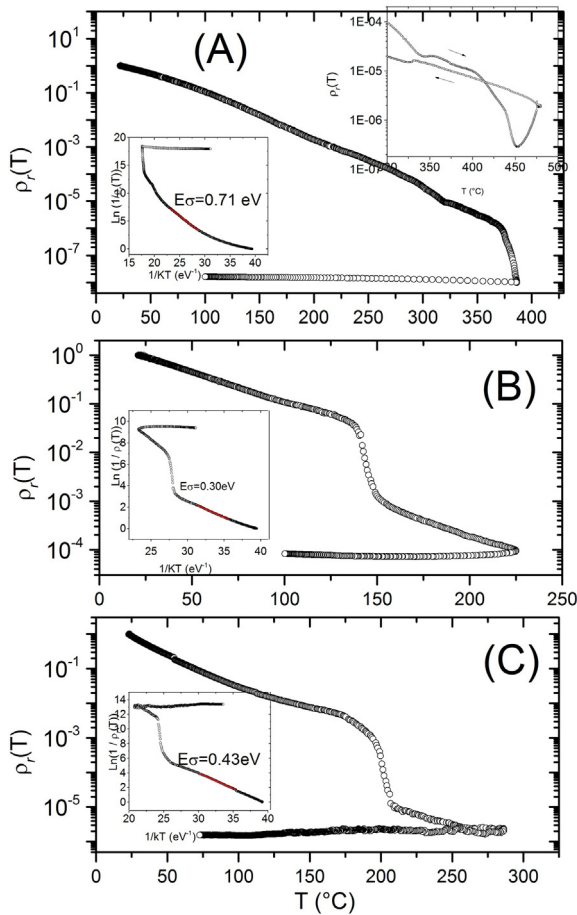


Fig. 5. XRD patterns obtained at RT after  $R_s$  vs.  $T$  measurements on  $\text{In}_{50}\text{Sb}_{15}\text{Te}_{35}$  (A), E1 (B) and E2 (C) films. The presence of Ag is due to rests of the electric contacts.

XRD pattern obtained after  $R_s(T)$  measurement, presented in Fig. 6C, shows that the crystallization products after a heating process of the film from RT to 290 °C followed by a free cooling back to RT are  $\text{In}_2\text{Te}_3$  and  $\text{In}_x\text{Sb}_{2-x}\text{Te}_3$ . Sb may also be present.

From the Arrhenius plot depicted in the inset, the activation energy of electric transport of the amorphous film can be determined as  $E_\sigma = 0.43$  eV.

#### 4. Discussion

On the basis of the reported results In-Sb-Te system does not possess a good ability for amorphization when melt-quenching technique is involved. Nevertheless, amorphous films are easily prepared by means of pulsed laser deposition (PLD) technique reproducing in the films the target stoichiometry. However, a low chalcogen loss may take place due to its relatively high vapor pressure. Nevertheless Te loss is in the order of 3% for  $\text{In}_{50}\text{Sb}_{15}\text{Te}_{35}$ , 1% for E1 and 2% for E2, in the same order as registered other authors [14,17]. Accordingly, PLD becomes an attractive tool for manufacturing 2D devices for PCM as an alternative technique to those commonly used such as metallorganic chemical vapor deposition [23] and co-sputtering [24].

$\text{In}_{50}\text{Sb}_{15}\text{Te}_{35}$  films crystallization products are InSb (302 °C) and InTe (320 °C) that, at 420 °C, react endothermically forming cubic  $\text{In}_3\text{SbTe}_2$ . This phase decomposes peritectically in the 530 °C–570 °C range. After melting at the end of the DSC scan the crystalline phases identified by XRD, once RT was achieved are  $\text{In}_3\text{SbTe}_2$  as well as InSb and InTe. On the other hand  $R_s$  falls eight orders of magnitude during the transformation of the amorphous onto the crystalline film both at RT passing through a maximum temperature of about 380 °C. In this case, the

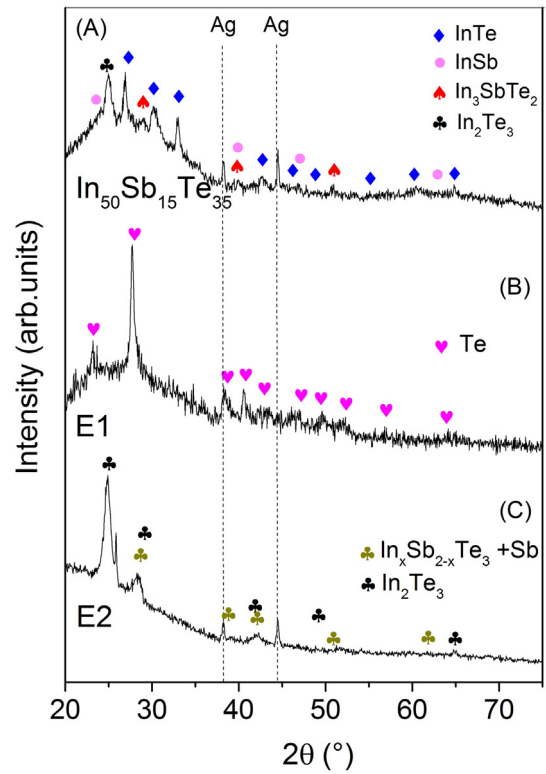


Fig. 6. XRD patterns obtained at RT after  $R_s$  vs.  $T$  measurements on  $\text{In}_{50}\text{Sb}_{15}\text{Te}_{35}$  (A), E1 (B) and E2 (C) films. The presence of Ag is due to rests of the electric contacts.

main crystallization products identified are InSb and InTe though traces of  $\text{In}_3\text{SbTe}_2$  are also detected. Finally, the wide peak corresponding to cubic  $\text{In}_2\text{Te}_3$  ( $a = 6.16$  Å) is probably due to heterogeneous nucleation of  $\text{In}_2\text{Te}_3$  on InSb ( $a = 6.48$  Å) that may be attributed to the fact that both phases are cubic, with the same space group ( $F-43m$ ) and a lattice mismatch of only about 6%. Nevertheless, no traces of In were detected.

The equilibrium phases forming E1 eutectic are Te,  $\text{In}_2\text{Te}_3$  and  $\text{In}_x\text{Sb}_{2-x}\text{Te}_3$  [20] whereas E1 ingot resulted to be consisted of Te,  $\text{In}_2\text{Te}_3$  and  $\text{In}_x\text{Sb}_{2-x}\text{Te}_3$ . This may be attributed to the fact that  $\text{In}_2\text{Te}_3$  is formed peritectically [25] and the synthesis of the sample needs special care so, failure to comply with all the required conditions, as in melt quenching case, could lead to  $\text{In}_2\text{Te}_3$  and Te instead of  $\text{In}_2\text{Te}_3$  [26].

E1 film crystallizes at 145 °C and melts at  $T_m \approx 400$  °C. After melting, the crystalline phases obtained by means of a cooling inside the DSC holder are Te and  $\text{In}_x\text{Sb}_{2-x}\text{Te}_3$ . From the analysis of Te pattern no significant volume contraction was registered relative to hexagonal Te pattern (PDF#36-1452). As no traces of  $\text{In}_2\text{Te}_3$  are detected and taking into account the high solubility of  $\text{In}_2\text{Te}_3$  in  $\text{Sb}_2\text{Te}_3$ , the stoichiometry of this rhombohedral phase may be assumed  $\text{In}_x\text{Sb}_{2-x}\text{Te}_3$  with  $x \sim 1$ . This interpretation is based not only on stoichiometry of E1, with similar concentration of In and Sb (about 8.3%), but also on the fact that the equilibrium solubility limit for  $\text{In}_2\text{Te}_3$  in  $\text{Sb}_2\text{Te}_3$  is, according to [20], about  $\text{In}_8\text{Sb}_{32}\text{Te}_{60}$  mole% at RT so, changing mole% to formula units  $3:60 = 2:40 = (2-x):32 = x:8$  ( $x = 0.4$ ) and about  $\text{In}_{20}\text{Sb}_{20}\text{Te}_{60}$  mol% at 600 °C that in formula units is  $3:60 = x:20 = (2-x):20$ , that is ( $x \sim 1$ ).

In the case of E1 films after DSC measurements, XRD patterns were analyzed and the lattice volume of, supposedly,  $\text{In}_x\text{Sb}_{2-x}\text{Te}_3$  was compared with pure  $\text{Sb}_2\text{Te}_3$  reference. The calculated lattice volume in this sample resulted 1.5% smaller than that of the reference. Since the stoichiometry of  $\text{In}_x\text{Sb}_{2-x}\text{Te}_3$  in E1 film after DSC scan is assumed  $\text{InSbTe}_3$ , the 1.5% lattice volume contraction relative to  $\text{Sb}_2\text{Te}_3$  in this sample is due to about a 50% molar dilution of  $\text{In}_2\text{Te}_3$  in antimony telluride phase, forming  $\text{InxSb}_{2-x}\text{Te}_3$ . On the other hand, the calculated volume contraction of  $\text{Sb}_2\text{Te}_3$  for E1 ingot was 0.8% and may be attributed to a lower solubility of  $\text{In}_2\text{Te}_3$  in  $\text{Sb}_2\text{Te}_3$ .

However, after  $R_s(T)$  measurement the unique crystalline phase identified is Te but a volume contraction of about 2% was estimated from the analysis of XRD pattern. This volume contraction may be attributed to the solid solubility of  $\text{In}_x\text{Sb}_{2-x}\text{Te}_3$  in Te. The sheet resistivity falls four orders of magnitude along the transformation of the amorphous onto a partially crystallized film passing through a maximum temperature of about 225 °C.

E2 ingot crystallization products were identified as  $\text{In}_x\text{Sb}_{2-x}\text{Te}_3$  and InSb plus Sb that cannot be clearly distinguished by XRD. This may be attributed to the formation of  $\text{In}_x\text{Sb}_{2-x}\text{Te}_3$ , involving all Te atoms and an undetermined amount of In atoms. The lack of free Te and the abundance of Sb favor the formation of InSb leaving aside the excess Sb.

E2 film crystallizes at 224 °C and after an endothermic reaction at 363 °C melts at 542 °C. The unique crystalline phase distinguished after solidification is non-equilibrium  $\text{In}_x\text{Sb}_{2-x}\text{Te}_3$ , that is rhombohedral  $\text{In}_x\text{Sb}_{2-x}\text{Te}_3$  involving all In and all Te atoms plus a fraction of Sb atoms. Considering the measured composition of E2,  $\text{In}_{10.34}\text{Sb}_{52.44}\text{Te}_{37.22}$  and turning to formula units results  $3:37.22 = x:10.34$  that is  $x = 0.8$  and  $2-x = 1.2$  then,  $x:10.34 = 1.2:\text{Sb}$  concentration that is 15.51 mol%. Accordingly  $\text{In}_{0.8}\text{Sb}_{1.2}\text{Te}_3$  involves all In and Te atoms plus 15.51 mol% of Te. The remaining free Sb is 36.93 mol%. An amount of about 36.93 mol% of Sb should also be present. Nevertheless, after  $R_s(T)$  measurement the crystalline phases identified are  $\text{In}_2\text{Te}_3$  and  $\text{In}_x\text{Sb}_{2-x}\text{Te}_3$ . However, the enlargement of the width of the peaks attributed to  $\text{In}_x\text{Sb}_{2-x}\text{Te}_3$  may be due to the presence of Sb as well.

After these facts we conclude that the endothermic transformation at 363 °C may be attributed to a solid state reaction of the above mentioned phases to form rhombohedral  $\text{In}_x\text{Sb}_{2-x}\text{Te}_3$ .

In the cases of E2 ingot and the films after  $R_s$  and DSC measurements, the corresponding XRD patterns were also analyzed and the lattice volumes of  $\text{In}_x\text{Sb}_{2-x}\text{Te}_3$  were compared with pure  $\text{Sb}_2\text{Te}_3$  reference. In all three samples, the calculated lattice volume resulted less than in the reference one. In particular, the lattice volume of  $\text{In}_x\text{Sb}_{2-x}\text{Te}_3$  in the case of the ingot sample resulted about 2.8% smaller, in the case of the film after  $R_s$  measurement the lattice volume contraction was about 2.4% and in the case of powdered film after DSC scan the corresponding volume was about 3.2% smaller than in the reference sample. The lattice volume reduction observed for all the analyzed samples can be explained by substitution of Indium atom for one of the atoms of  $\text{Sb}_2\text{Te}_3$  phase [27]. And the degree of the substitution in these samples is, apparently, different. In the case of E2 film after DSC scan where the stoichiometry of  $\text{In}_x\text{Sb}_{2-x}\text{Te}_3$  is considered  $\text{In}_{0.8}\text{Sb}_{1.2}\text{Te}_3$  we assume that a 3.2% lattice volume contraction relative to the reference  $\text{Sb}_2\text{Te}_3$  is due to a total Indium dilution in antimony telluride phase, as was the case of E1 film. On the other hand, a smaller lattice volume contraction of  $\text{In}_x\text{Sb}_{2-x}\text{Te}_3$  phase in the ingot E2 (2.8%) and E2 film after  $R_s$  measurement may indicate a partial Indium dilution in the mentioned binary phase since InSb and  $\text{In}_2\text{Te}_3$  were identified, respectively, in the above mentioned samples. Particularly in the second case, where the stoichiometry of  $\text{In}_x\text{Sb}_{2-x}\text{Te}_3$  may be supposed not far from the equilibrium one ( $\text{In}_{0.4}\text{Sb}_{1.6}\text{Te}_3$ ), we assume that the corresponding volume reduction of 2.4%, relative to the reference, is due to the dilution of 20 mol% of  $\text{In}_2\text{Te}_3$  in antimony telluride.

Nevertheless, although the results for E1 and for E2 present internal coherence, they cannot be incorporated in a single model, probably due to the presence of a different third phase that is Te for E1 and Sb for E2 that may also contribute to modify  $\text{In}_x\text{Sb}_{2-x}\text{Te}_3$  lattice.

Along  $R_s(T)$  measurement cycle whose maximum temperature was about 290 °C,  $\rho_r(T)$  falls about six orders of magnitude from an amorphous to a crystallized film, both at RT. The transport behavior of the crystallized film is semiconducting at high temperature but metallic below 200 °C. This behavior may be attributed to the presence of Sb, not distinguished from  $\text{In}_x\text{Sb}_{2-x}\text{Te}_3$  by means of XRD.

On the other hand, as in most chalcogenide glasses, the abundance of defects fixes the Fermi energy in the middle of the forbidden gap [28] so, the activation energy of conductivity may be associated to a half of the

mobility gap [29]. Accordingly, the mobility gap values result 1.42 eV, 0.60 eV and 0.86 eV for  $\text{In}_{50}\text{Sb}_{15}\text{Te}_{35}$ , E1 and E2 amorphous films, respectively. These values are in good agreement with mobility gap values reported by other authors for binary chalcogenide glasses of the III-V, III-VI V-VI families. For instance, Tanaka [30] mentioned a mobility gap of 2.8 eV for glassy  $\text{As}_2\text{S}_3$  whereas for  $\text{As}_2\text{Se}_3$  Zakery and Elliott [31] attribute a mobility gap of 1.1 eV and for  $\text{As}_2\text{Te}_3$  glasses Weiser and Brodsky attribute a mobility gap of 0.8 eV [32]. For glassy InSb Eckenbach et al. [33] reported a band gap of 0.65 eV and for  $\text{In}_2\text{Te}_3$  [34] reported one of 1.04 eV. On the other hand, single phase  $\text{Ga}_6\text{Sb}_5\text{Te}$  has a band gap  $E_g = 0.65$  eV [35].

In order to evaluate the performance of each composition to be applied to PCM, some parameters should be compared:  $T_c$ , crystallization products after  $R_s(T)$  measurements, the measured temperature range ( $T_{max}$ ),  $\rho_r(T)$  fall from amorphous at RT to crystallized sample at RT calculated as  $\Delta\rho_r(RT) = \rho_r(RT)_{AMORPHOUS} - \rho_r(RT)_{CRYSTAL}$ , solid state (SS) reaction temperature ( $T_{ss}$ ), if any, SS reaction products and  $T_m$ , either eutectic  $T_E$  or  $T_P$  peritectic.

As it can be seen,  $\text{In}_{50}\text{Sb}_{15}\text{Te}_{35}$  amorphous film crystallizes into two phases, namely, InSb and InTe and this happens at two different temperatures (302 °C and 320 °C approximately). The marginal amount of  $\text{In}_3\text{SbTe}_2$  may be controlled with  $T_{max}$  in order to restrict the crystalline phases to those that are in equilibrium at RT. On the other hand if heating advances to higher temperatures,  $\text{In}_{50}\text{Sb}_{15}\text{Te}_{35}$  offers additional features that enables the potential of its application to multilevel data storage. Unlike that film, E1 amorphous film presents a primary crystallization of Te that is the only crystalline phase detected after the  $R_s(T)$  measurement cycle. However, the volume contraction detected let us suppose that Te incorporated In and Sb in solid solution. Further study is required to evaluate its crystallization process and the stability of the crystallization product.

E2 film's  $T_c \approx 225$  °C is considerably higher than the one corresponding to E1 film. In its turn, that temperature is not as high as the  $T_c$  corresponding to  $\text{In}_{50}\text{Sb}_{15}\text{Te}_{35}$  film. The  $T_c$  of E2 seems to be reasonable for practical purposes. It avoids unnecessary overheating of the memory device and in its turn is also favorable from the point of view of energy cost. On the other hand, it is more stable in its amorphous state than E1 or, even  $\text{Ge}_2\text{Sb}_2\text{Te}_5$  ( $T_c \approx 120\text{--}160$  °C [36]) and also in its final state as the crystallization products  $\text{In}_2\text{Te}_3$  and  $\text{In}_x\text{Sb}_{2-x}\text{Te}_3$  are equilibrium phases at RT.

The maximum temperatures involved in these processes are chosen according to the  $T_c$  with the aim to observe a resounding fall in  $\rho_r$ . The best choice seems to be  $T_{max}$ , not far from  $T_c$ . Accordingly,  $T_{ss}$  either for IST or for E2 are out of the temperature range measured.

The melting transformation for IST corresponds to a peritectic reaction, that is, about a half of our sample melts whereas the rest of the sample remains solid with a composition not far from InTe. As temperature increases, the liquid phase composition changes from the peritectic composition of about  $\text{In}_5\text{Sb}_3\text{Te}_2$  (60 mol% IST) towards  $\text{In}_3\text{SbTe}_2$  at the expenses of solid state InTe [13]. The later solidification to obtain an amorphous must roll back this process. Accordingly, the process of obtaining amorphous starting from the crystalline sample will not be too fast. On the other hand, the  $T_m$  of E1 and E2 correspond to eutectic points but, while E1 is not very well defined, E2 presents a single thin endothermic peak. Because of this property, eutectic film E2 presents some advantage with respect to  $\text{In}_{50}\text{Sb}_{15}\text{Te}_{35}$  (or IST) or even to E1 for memory storage.

Finally, the jumps developed by  $\rho_r(T)$  for all three samples are adequate for distinguishing undoubtedly between a resistive state and a conductive state. As the phases obtained after crystallization are equilibrium phases at RT, the conductive state may be associate to the information storage, and may be read as ON, whereas the resistive state may be read as an OFF state. This map of points ON and OFF encodes the stored information.

The present results, thermal ( $T_c$ ,  $T_m$ ,  $T_{ss}$ , crystallization products), structural and electrical, are in concordance with those of other authors

already mentioned along the text, particularly (but not only) those of references [14–18].

Further investigations of these films are in progress.

## 5. Conclusions

In search of suitable materials for phase change memories, we have prepared amorphous thin films of In-Sb-Te system by PLD. We explored three stoichiometries:  $\text{In}_{50}\text{Sb}_{15}\text{Te}_{35}$  (not far from  $\text{In}_3\text{SbTe}_2$ ) and two eutectics such as  $\text{In}_8\text{Sb}_8\text{Te}_{84}$  (E1) and  $\text{In}_{10}\text{Sb}_{51}\text{Te}_{39}$  (E2). Sheet resistivity ratio  $\rho_r(T)$  of the films revealed, for all the three samples, an abrupt jump of several orders of magnitude that allows to distinguish undoubtedly a high resistance state for amorphous at RT and a low resistance state for crystallized samples. From the above mentioned results the mobility gap of the glasses of the three studied compositions were calculated (1.42 eV, 0.60 eV and 0.86 eV for amorphous  $\text{In}_{50}\text{Sb}_{15}\text{Te}_{35}$ , E1 and E2, respectively). In agreement with  $\rho_r(T)$  scan DSC allowed identifying the  $T_c$  of the films. Additionally, DSC allowed the determination of solid state reaction temperatures for  $\text{In}_{50}\text{Sb}_{15}\text{Te}_{35}$  and E2 and the  $T_m$  for all samples.

From the thermal point of view, the eutectic E2 ( $\text{In}_{10}\text{Sb}_{51}\text{Te}_{39}$ ) with  $T_c = 224$  °C and  $T_m = 542$  °C, seems to be an attractive candidate for its use in phase change memories. From the electrical point of view,  $\rho_r(T)$  falls 6 orders of magnitude between an amorphous and a crystal, both at RT. Particularly, the fact that the crystallization towards two stable phases takes place in a lapse of 30 °C with a change in  $\rho_r(T)$  of about 3 orders of magnitude reinforces the above mentioned potentiality. Nevertheless, due to their good electrical characteristics, the other compositions cannot be discarded.

The evaluation of new compositions out of InSb-InTe tie line, the study of the unusual solubility that evidenced several phases of this system and the analysis of eutectics potentiality for PCM is our contribution to the knowledge of In-Sb-Te system.

## Acknowledgements

We thank Universidad de Buenos Aires (Project 20020130100647BA), CONICET (PIP 11220120100541) and ANPCyT (PICT08-1314) for their financial support. We are grateful to Dr. Faigon for having facilitated the equipment employed for electrical measurements.

## References

- [1] S.R. Ovshinsky, Reversible electrical switching phenomena in disordered structures, *Phys. Rev. Lett.* 21 (1968) 1450, <http://dx.doi.org/10.1103/PhysRevLett.21.1450>.
- [2] E.J. Evans, J.H. Helbers, S.R. Ovshinsky, Reversible conductivity transformations in chalcogenide alloy films, *J. Non-Cryst. Solids* 2 (1970) 334, [http://dx.doi.org/10.1016/0022-3093\(70\)90149-3](http://dx.doi.org/10.1016/0022-3093(70)90149-3).
- [3] Y. Maeda, H. Andoh, I. Ikuta, H. Minemura, Reversible phase-change optical data storage in InSbTe alloy films, *J. Appl. Phys.* 64 (4) (1988) 1715, <http://dx.doi.org/10.1063/1.342502>.
- [4] L. Men, F. Jiang, F. Gan, Short-wavelength phase-change optical data storage in In-Sb-Te alloy films, *Mater. Sci. Eng.* B47 (1997) 18, [http://dx.doi.org/10.1016/S0921-5107\(97\)02042-4](http://dx.doi.org/10.1016/S0921-5107(97)02042-4).
- [5] M. Imran, O.A. Lafi, M. Abu-Samak, Effect of thermal annealing on some electrical properties and optical band gap of vacuum evaporated Se 65 Ga 30 In 5 thin films, *Vacuum* 86 (2012) 1589, <http://dx.doi.org/10.1016/j.vacuum.2012.03.021>.
- [6] Y.T. Kim, S.-I. Kim, Comparison of thermal stabilities between Ge-Sb-Te and In-Sb-Te phase change materials, *Appl. Phys. Lett.* 103 (2013) 121906, <http://dx.doi.org/10.1063/1.4821855>.
- [7] Y. Zou, O.O. Ogbuu, L. Li, S. Danto, S. Novak, J. Novak, J.D. Musgraves, K. Richardson, J. Hu, Effect of annealing conditions on the physico-chemical properties of spin-coated As 2 Se 3 chalcogenide glass films, *Opt. Mater. Express* 2 (12) (2012) 1723, <http://dx.doi.org/10.1364/OME.2.001723>.
- [8] P. Nèmec, V. Nazabal, A. Moreacc, J. Gutwirth, L. Beneš, M. Frumar, Effect of annealing conditions on the physico-chemical properties of spin-coated As 2 Se 3 chalcogenide glass films, *Mater. Chem. Phys.* 136 (2012) 935, <http://dx.doi.org/10.1016/j.matchemphys.2012.08.024>.
- [9] A. Ureña, A. Piarristeguy, M. Fontana, C. Vigreux-Bercovici, A. Pradel, B. Arcondo, Characterisation of thin films obtained by laser ablation of Ge 28 Se 60 Sb 12 glasses, *J. Phys. Chem. Solids* 68 (2007) 993, <http://dx.doi.org/10.1016/j.jpcs.2007.03.021>.
- [10] S. Song, N. Carlie, J. Boudies, L. Petit, K. Richardson, C.B. Arnold, Spin-coating of Ge 23 Sb 7 S 70 chalcogenide glass thin films, *J. Non-Cryst. Solids* 355 (2009) 2272, <http://dx.doi.org/10.1016/j.jnoncrysol.2009.07.015>.
- [11] N. Yamada, Origin, secret, and application of the ideal phase-change material GeSbTe, *Phys. Status Solidi B* 249 (No. 10) (2012) 1837–1842, <http://dx.doi.org/10.1002/pssb.201200618>.
- [12] T. Matsunaga, Y. Umetani, N. Yamada, Structural study of a Ag 3.4 In 3.7 Sb 76.4 Te 16.5 quadruple compound utilized for phase-change optical disks, *Phys. Rev. B* 64 (2001) 184116, <http://dx.doi.org/10.1103/PhysRevB.64.184116>.
- [13] M. Wüttig, N. Yamada, Phase-change materials for rewritable data storage, *Nat. Mater.* 6 (2007) 824, <http://dx.doi.org/10.1038/nmat2009>.
- [14] T. Schröder, T. Rosenthal, S. Grott, C. Stiewe, J. de Boor, O. Oeckler, Disorder and transport properties of In3SbTe2 – an X-ray, neutron and electron diffraction study, *Z. Anorg. Allg. Chem.* 639 (14) (2013) 2536, <http://dx.doi.org/10.1002/zaac.201300317>.
- [15] T. Matsunaga, N. Yamada, Y. Kubota, Structures of stable and metastable Ge2Sb2Te5, an intermetallic compound in GeTe-Sb2Te3 pseudobinary systems, *Acta Cryst. B* 60 (2004) 685, <http://dx.doi.org/10.1107/S0108768104022906>.
- [16] E.T. Kim, J.Y. Lee, Y.T. Kim, Investigation of electrical characteristics of the In3Sb1Te2 ternary alloy for application in phase-change memory, *Phys. Status Solidi RRL* 3 (2009) 103, <http://dx.doi.org/10.1002/pssr.200903049>.
- [17] L. Hromádka, J. Prikryl, L. Strizik, P. Košťál, L. Beneš, M. Frumar, Physico-chemical properties of Sb-rich (Sb, In)-Te thin films, *J. Alloys Compd.* 617 (2014) 306, <http://dx.doi.org/10.1016/j.jallcom.2014.07.110>.
- [18] K. Kifune, Y. Kubota, T. Matsunaga, N. Yamada, Extremely long period-stacking structure in the Sb-Te binary system, *Acta Cryst. B* 61 (2005) 492, <http://dx.doi.org/10.1107/S0108768105017714>.
- [19] Maud - Materials Analysis Using Diffraction. (<http://www.ing.unitn.it/~maud/download.html>)
- [20] B. Legendre, B. Gather, R. Blachnik, Ternary chalcogen systems. IX. – The system indium – antimony – tellurium, *Z. Metallkd./Mater. Res. Adv. Tech.* 71 (9) (1980) 588.
- [21] K. Deneke, A. Rabenau, Über die Natur der Phase In3SbTe2, mit Kochsalzstruktur, *Z. Anorg. Allg. Chem.* 333 (1964) 201, <http://dx.doi.org/10.1002/zaac.19643330406>.
- [22] Y.T. Kim, E.T. Kim, J.Y. Lee, Characteristics of InSbTe phase-change random access memory, *Proceedings of the 13th WSEAS International Conference on CIRCUITS* 2009, p. 203.
- [23] T. Stoycheva, M. Longo, R. Fallica, F. Volpe, C. Wiemer, Growth study and characterization of In-Sb-Te compounds deposited onto different substrates by metal-organic chemical vapour deposition, *Thin Solid Films* 533 (2013) 66, <http://dx.doi.org/10.1016/j.tsf.2012.10.107>.
- [24] Y.M. Lee, D.D. Dung, S. Cho, M.S. Jung, D.K. Choi, D. Ahn, M.K. Kim, J.-Y. Kim, M.-C. Jung, Characterization of Fe-doped In-Sb-Te (Fe: 10 at%) material with individual electrical-phase-change and magnetic properties, *AIP Adv.* 1 (2011) 022150, <http://dx.doi.org/10.1063/1.3609265>.
- [25] V.P. Zlomanov, M.S. Sheiman, B. Legendre, Phase diagram and thermodynamic properties of phases in the In-Te system, *J. Phase Equilib.* 22 (3) (2001) 339, <http://dx.doi.org/10.1361/105497101770338851>.
- [26] E.G. Lavut, N.V. Chelovskaya, G.A. Qispe Paukar, V.N. Demin, V.P. Zlomanov, The standard molar enthalpy of formation of indium telluride In 2 Te 5, *J. Chem. Thermodyn.* 29 (1997) 811, <http://dx.doi.org/10.1006/jcht.1997.0209>.
- [27] A.J. Rosenberg, A.J. Strauss, Solid solutions of In 2 Te 3 in Sb 2 Te 3 and Bi 2 Te 3, *J. Phys. Chem. Solids* 19 (1961) 105, [http://dx.doi.org/10.1016/0022-3697\(61\)90063-4](http://dx.doi.org/10.1016/0022-3697(61)90063-4).
- [28] N.F. Mott, E.A. Davis, *Electronic Processes in Non-crystalline Materials*, second ed. Clarendon Press, Oxford, 1979 466.
- [29] A. Kolobov, J. Tominaga, Springer Series en Materials Science, Vol.164, Chalcogenides, Metastability and Phase Change Phenomena Springer-Verlag Berlin Heidelberg 2012, p. 26, <http://dx.doi.org/10.1007/978-3-642-28705-3>.
- [30] K. Tanaka, Have we understood the optical absorption edge in chalcogenide glasses? *J. Non-Cryst. Solids* 431 (2016) 21, <http://dx.doi.org/10.1016/j.jnoncrysol.2015.03.006>.
- [31] A. Zakery, S.R. Elliott, *Optical Nonlinearities in Chalcogenide Glasses and Their Applications*, Springer-Verlag Berlin Heidelberg, 2007 6.
- [32] K. Weiser, M.H. Brodsky, dc conductivity, optical absorption, and photoconductivity of amorphous arsenic telluride films, *Phys. Rev. B* 1 (2) (1970) 791, <http://dx.doi.org/10.1103/PhysRevB.1.791>.
- [33] W. Eckenbach, W. Fuhs, J. Stuke, Preparation and electrical properties of amorphous InSb, *J. Non-Cryst. Solids* 5 (1971) 264, [http://dx.doi.org/10.1016/0022-3093\(71\)90035-4](http://dx.doi.org/10.1016/0022-3093(71)90035-4).
- [34] Indium Telluride Cylinder Fiber Laser; Abhinay Sandupatia, Master Thesis Syracuse University, USA (2014); A. Sandupatia, J. Flattery; Ph. Kornreich, *Opt. Eng.* 54, 126113 (2015) <http://dx.doi.org/10.1117/1.OE.54.12.126113>
- [35] K. Kurata, T. Hirai, Semiconducting properties of several III BV-BVI B ternary materials and their metallurgical aspects, *Solid State Electron.* 9 (1966) 633, [http://dx.doi.org/10.1016/0038-1101\(66\)90007-4](http://dx.doi.org/10.1016/0038-1101(66)90007-4).
- [36] N. Yamada, E. Ohno, K. Nishiuchi, N. Akahira, M. Takao, Rapid-phase transitions of GeTe-Sb2Te3 pseudobinary amorphous thin films for an optical disk memory, *J. Appl. Phys.* 69 (1991) 2849, <http://dx.doi.org/10.1063/1.348620>.